UC Irvine

UC Irvine Previously Published Works

Title

Hip load capacity and yield load in men and women of all ages

Permalink

https://escholarship.org/uc/item/0bc1r8f7

Authors

Keyak, JH

Kaneko, TS

Khosla, S

et al.

Publication Date

2020-08-01

DOI

10.1016/j.bone.2020.115321

Peer reviewed

eScholarship.org Powered by the California Digital Library
University of California

Hip Load Capacity and Yield Load in Men and Women of All Ages

J.H. Keyak [a,b,c,*], T.S. Kaneko [a], S. Khosla [d], S. Amin [e,f], E.J. Atkinson [g], T.F. Lang [h],

J.D. Sibonga [i]

March 2, 2020

[a]Department of Radiological Sciences, University of California, Irvine, CA, USA

[b]Department of Biomedical Engineering, University of California, Irvine, CA, USA

[c]Department of Mechanical and Aerospace Engineering, University of California, Irvine, CA, USA

[d]Division of Endocrinology, Department of Medicine, Mayo Clinic, Rochester, MN, USA

[e]Division of Epidemiology, Department of Health Sciences Research, Mayo Clinic, Rochester, MN, USA

[f]Division of Rheumatology, Department of Medicine, Mayo Clinic, Rochester, MN, USA

[g]Division of Biomedical Statistics and Informatics, Department of Health Sciences Research, Mayo Clinic, Rochester, MN, USA

[h]Department of Radiology and Biomedical Imaging and School of Dentistry, University of California, San Francisco, CA, USA

[i]Division of Biomedical Research and Environmental Sciences, NASA Lyndon B. Johnson Space Center, Houston, TX, USA

*Corresponding author: Joyce H. Keyak, PhD, Department of Radiological Sciences, University of California, Irvine, CA 92697-5000. Phone: 949-824-9421; Fax: 949-824-8115; Email: jhkeyak@uci.edu.

Abstract

Quantitative computed tomography (QCT) based finite element (FE) models can compute subject-specific proximal femoral strengths, or fracture loads, that are associated with hip fracture risk. These fracture loads are more strongly associated with measured fracture loads than DXA and QCT measures and are predictive of hip fracture independently of DXA bone mineral density (BMD). However, interpreting FE-computed fracture loads of younger subjects for the purpose of evaluating hip fracture risk in old age is challenging due to limited reference data. The goal of this study was to address this issue by providing reference data for male and female adult subjects of all ages. QCT-based FE models of the left proximal femur of 216 women and 181 men, age 27 to 90 years, from a cohort of Rochester, MN residents were used to compute proximal femoral load capacity in single-limb stance and posterolateral fall loading (Stance_LC and Fall_LC, respectively) [US Patent No. 9,245,069] and yield load under fall loading (Fall_yield). To relate these measures to information about hip fracture, the CT scanner and calibration phantom were cross-calibrated with those from our previous prospective study of hip fracture in older fracture and control subjects, the Age Gene/Environment Susceptibility (AGES) Reykjavik cohort. We then plotted Stance_LC, Fall_LC and Fall_yield versus age for the two cohorts on the same graphs. Thus, proximal femoral strengths in individuals above 70 years of age can be assessed through direct comparison with the FE data from the AGES cohort which were analyzed using identical methods. To evaluate younger individuals, reductions in Stance_LC, Fall_LC and Fall_yield from the time of evaluation to age 70 years can be cautiously estimated from the average yearly cross-sectional decreases found in this study (108 N, 19.4 N and 14.4 N, respectively, in men and 120 N, 19.4 N and 21.6 N, respectively, in women), and the projected fracture loads can be compared with data from the AGES cohort. Although we did not set specific thresholds for identifying individuals at risk of hip fracture, these data provide some guidance and may be used to help establish diagnostic

criteria in future. Additionally, given that these data were nearly entirely from Caucasian subjects, future research involving subjects of other races/ethnicities is necessary.

Keywords

hip fracture; femur; bone strength; finite element analysis; osteoporosis; quantitative computed tomography

Abbreviations

FE	finite element
Stance_LC	finite element analysis-computed proximal femoral load capacity in single-limb stance loading
Fall_LC	finite element analysis-computed proximal femoral load capacity for loading representing a fall onto the posterolateral aspect of the greater trochanter.
Fall_yield	finite element analysis-computed proximal femoral yield load for a fall onto the posterolateral aspect of the greater trochanter.

Introduction

Fracture of the proximal femur is a devastating consequence of inadequate proximal femoral whole bone strength which can occur from bone loss or problems experienced during development. Although treatments to slow loss and/or increase proximal femoral strength exist, identifying patients who are at long-term risk of fracture and need treatment is challenging. Dual-energy X-ray absorptiometry (DXA) has long been used clinically to evaluate areal bone mineral density (BMD) and bone mineral content (BMC) in the femoral neck, and total proximal femur. Although low areal BMD is statistically associated with an increased risk of hip fracture, DXA BMD cannot precisely distinguish between subjects who are at risk of fracture and those who are not, especially in those with intermediate BMD or osteopenia [1-4]. The two-dimensional nature of DXA is an inherent limitation that prevents separate assessment of cortical and trabecular bone, which makes early diagnosis problematic. During aging and unloading, bone loss is greater in trabecular than in cortical bone, but the presence of dense cortical bone dominates measurements of DXA areal BMD which causes changes in trabecular BMD to be obscured [5-6]. Quantitative computed tomography (QCT), a three-dimensional technique for measuring BMD, offers a solution to this particular problem while providing additional benefits. Not only can QCT separately evaluate trabecular and cortical volumetric BMD and BMC, it can also provide measures of trabecular and cortical bone volume and geometry. Studies have shown that QCT measures can assess hip fracture risk independently of DXA BMD [7-9].

Although DXA and QCT measures are helpful for evaluating regional BMD and BMC, these techniques cannot capture complex three-dimensional geometrical and structural factors, such as the heterogeneous distribution of bone density, and variations in cortical thickness that influence hip fracture risk [10]. As with failure of any structure, fracture of the proximal femur occurs when an applied force (i.e. load) exceeds the structure's ability to support that load (i.e. its load capacity). If the load capacity of the proximal femur is sufficient to withstand the loads

that it typically encounters, the risk of proximal femur fracture will be low. With that rationale, the present study focuses on an individual's proximal femur load capacity as a biomechanical indicator of hip fracture risk. This load capacity can be calculated through use of CT scan-based finite element (FE) modeling, a robust biomechanical tool that can account for a subject's individual proximal femoral geometry and three-dimensional bone density distribution. Thus, rather than using BMD as a bone health measure that is statistically associated with fracture risk, CT scan-based FE modeling constructs a biomechanical representation of the proximal femur that computes the minimum force required to cause fracture.

Previous studies have shown that QCT-based FE-computed proximal femoral strength, or fracture load, is more strongly associated with measured fracture load than DXA and QCT measures [11-13] and is predictive of hip fracture independently of DXA BMD [14-16]. However, the current challenge of employing FE models to assess hip fracture risk is interpreting the FE model results. Although we would ideally compare a patient's FE model load capacity with the loads the proximal femur experiences, these loads are too uncertain to obtain useful fracture predictions. As an alternative, we can compare a patient's FE load capacity with those of subjects who have and have not had hip fractures. If a patient's load capacity is greater than that of most subjects who have had hip fractures, we could conclude that the risk of fracture is comparatively low. On the other hand, if a patient's load capacity is comparable to that of many subjects who have had hip fractures and less than that of subjects who have not had hip fractures, we would conclude that the patient is at relatively high risk of hip fracture. Unfortunately, the limitation of this approach is that most previous FE studies have focused on older subjects [14-19], making it difficult to evaluate patients early in life, while there is still time to treat and/or prevent bone loss due to aging, medical treatments (e.g. glucocorticoids or cancer treatment), spaceflight, congenital conditions or other factors. Therefore, the purpose of this study is to provide the reference data and guidance that will allow CT scan-based FE

models of the proximal femur to be used to evaluate proximal femoral load capacity of adult male and female subjects of all ages.

Methods

Subject and Imaging Data

We obtained anonymized QCT scans of the hips of 216 women and 181 men [mean age (range): 60.9 (27 to 90) years, and 59.9 (28 to 90) years, respectively] from the year 6 follow-up visit of a previous longitudinal study of an age-stratified random sample of Rochester, MN residents [20]. The subjects included here are a subset of that study and were selected because they had obtained both QCT scans and DXA scans at the year 6 follow-up time point. Subjects previously provided written informed consent that extended to the analyses presented here. Ninety-five percent of the men and 99% of the women were white. Thirty-five percent of the men and 32% of the women were obese as defined by a weight greater than 30% of the ideal weight for their height. Ninety-nine (46%) postmenopausal women had received estrogen therapy and 35 (16%) women and 3 (2%) men had received bisphosphonate therapy at some time prior to the scan. Although there were initially no exclusion criteria in the sample, data from 6 women and 5 men were excluded because CT scan image quality, presence of a prosthesis (6 subjects), or femoral head deformity (1 subject) prevented valid analysis, leaving 397 subjects (the Mayo cohort) for this study.

The QCT scans (Siemens, Sensation 64, 120kVp; 2-mm-thick slices; pixel size, 0.742 mm to 0.977 mm; convolution kernel, B30s) included a K_2HPO_4 calibration phantom (Model 3, Mindways Software, Inc., San Francisco, CA, USA), which was used to determine the K_2HPO_4 equivalent mineral density of each voxel (ρ_K, g/cm^3). Inclusion of this phantom in the image with the subject is necessary to correct for the effects of variable subject size and composition, and other factors that can influence the CT Hounsfield units. The 2-mm-thick slices were converted to 3-mm-thick slices for consistency with previous FE studies [14,18,21,22].

Fourier interpolation was performed over groups of three contiguous 2-mm-thick images to obtain six 1mm-thick contiguous images, followed by decimation (by averaging voxels in successive slices) to create two 3-mm-thick contiguous images.

To enable direct comparison of the data from this investigation with that from our previous prospective study of hip fracture, the Age Gene/Environment Susceptibility (AGES) Reykjavik cohort [5,14,18], which used a Siemens, Sensation 4 scanner and a calcium hydroxyapatite (CHA) phantom, we cross-calibrated the CT scanners of the two studies. A custom anthropometric hip phantom simulating the pelvic area of the human body [23] was imaged on each of the CT scanners using the settings and calibration phantom that were used when scanning subjects at that site. The calibration phantom at each site was used to measure the QCT density of the anthropometric phantom in terms of K_2HPO_4 or CHA equivalent density, as applicable, and these QCT densities were then related to the actual density measurements of the anthropometric calibration phantom. These relationships were then used to determine a cross-calibration relationship between ρ_K on the Rochester scanner and the QCT CHA equivalent density (ρ_{CHA}, g/cm^3) on the AGES scanner. This relationship was then applied at the voxel level to convert ρ_K obtained in Rochester to the CHA density equivalent to that obtained in the AGES study.

Nonlinear FE models of the left proximal femur of each subject were used to compute proximal femoral load capacity in two loading conditions, one representing single-limb stance and one representing impact from a fall onto the posterolateral aspect of the greater trochanter (Stance_LC and Fall_LC, respectively) [US Patent No. 9,245,069][24]. As an additional measure of proximal femoral integrity, linear FE models were used to evaluate the yield load (i.e. the load at the onset of fracture) under fall loading (Fall_yield). Linear FE models of stance loading were not used because they could not predict measured fracture loads precisely [22].

For each subject, FE models of the left proximal femur were generated as follows. The CT scan images were segmented by one of the authors (TSK) using thresholding combined with an

edge following algorithm [25] that was integrated with in-house software to create a user-interactive semi-automated segmentation procedure. The mesh was generated using linear 8-node cube-shaped elements measuring 3mm on a side [26]. Material properties of the elements were computed from ρ_K of each voxel in the element, which was converted to ρ_{CHA} using the CT scanner cross calibration equation described above. The resulting ρ_{CHA} of each voxel was then used to compute ash density (ρ_{ash}, g/cm^3): $\rho_{ash}=0.88703\rho_{CHA} + 0.063343$ [21,27-28]. Finally, ρ_{ash} was used to compute an isotropic elastic modulus (E) and yield strength (S), which was assumed to be equal to the ultimate strength, for each voxel (Table 1) [14,21]. If the calculated value of ρ_{ash} was less than zero, E and S were set equal to zero. The E and S of each element were then computed by averaging the respective values over all voxels in the element, while accounting for partial volume effects by scaling by the volume fraction of each voxel within the element. Poisson's ratio was set to 0.4 [22,29-30].

The material properties of each finite element were specified by assigning a material definition to the element. Elements with a computed elastic modulus below 5 MPa were assigned a material with E=0.01 MPa (essentially zero). The subsequent material moduli that were used to define the element properties increased by 5%, with $E = 5.125 \times (1.05)^{n-2}$ MPa, where n=2,3,…[22]. Thus, the error introduced by grouping properties into specific materials was less than 2.5%. The elastic moduli of the materials formed the basis for the nonlinear FE models.

Table 1. Material properties used in linear and nonlinear finite element models.

	Linear Fall	Nonlinear Stance		Nonlinear Fall	
Parameter	All Densities	Trabecular Bone ($\rho_{ash} \leq 0.6037$ g/cm^3)	Cortical Bone ($\rho_{ash} > 0.6037$ g/cm^3)	Trabecular Bone ($\rho_{ash} \leq 0.6037$ g/cm^3)	Cortical Bone ($\rho_{ash} > 0.6037$ g/cm^3)
E (MPa)	$14900\ \rho_{ash}^{1.86}$	$14900\ \rho_{ash}^{1.86}$		$14900\ \rho_{ash}^{1.86}$	$14900\ \rho_{ash}^{1.86}$
S (MPa)	$102\ \rho_{ash}^{1.80}$	$102\ \rho_{ash}^{1.80}$		$102\ \rho_{ash}^{1.80}$	23.9
ε_{AB}		$0.00189 + 0.0241\ \rho_{ash}$	$0.0184 - 0.0100\ \rho_{ash}$	0	
ε_{AB}'[a]		$(15/3)\ \varepsilon_{AB}$		0	
E_p (MPa)		$-2080\ \rho_{ash}^{1.45}$	−1000	$-125{,}000\rho_{ash}^{1.45}$	−60,200
E_p'(MPa) [a]		$(3\ E\ E_p) / (15\ E - 12\ E_p)$		$(3\ E\ E_p) / (15\ E - 12\ E_p)$	
σ_{min} (MPa)		$43.1\ \rho_{ash}^{1.81}$		0.42 S	

[a] The formulae for ε_{AB}' and E_p' represent adjustments to ε_{AB} and E_p that account for the difference between the size of the finite elements (3mm) and the size of the specimens in which these post-yield parameters were measured (15 mm) [31]. The equations for trabecular bone were applied to cortical bone as well.

The nonlinear FE models were designed to behave much like a mechanical testing experiment under displacement control. Displacement was incrementally applied to the femoral head and the resulting reaction force values on the femoral head initially increased, reached a peak value (the proximal femoral strength), and then decreased. To achieve this mechanical behavior, the post-yield material properties for each material were represented by an initial perfectly plastic phase at stress S until the plastic strain was ε_{AB}', followed by a strain softening phase with plastic modulus E_p' until the stress was σ_{min}, followed by an indefinite perfectly plastic phase [14,21,31]. Given that bone is anisotropic and these models employed isotropic properties, the post-yield properties had to be adjusted to obtain accurate proximal femoral fracture loads in different loading conditions. Thus, anisotropy was accounted for by employing different material strengths and post-yield properties in stance versus fall loading (Table 1).

The elastic modulus of each material was used as the basis for calculating the post-yield material properties. Many of the post-yield properties depended on ρ_{ash}, so the effective ρ_{ash} for each material was first calculated from the equation between E and ρ_{ash} (Table 1, $\rho_{ash}=(E/14900)^{(1/1.86)}$). The post-yield properties for each material were then calculated using the material's ρ_{ash} and the equations in Table 1 [14,21,31]. Thus, the linear elastic and nonlinear post-yield mechanical properties described a simplified, density-dependent, nonlinear stress-strain curve for each material and its corresponding element(s) [14,21].

Material yield was defined using the distortion energy theory, so element yield occurred when the FE-computed von Mises stress in the element exceeded the strength of the element, S. After yield, plastic flow was modeled assuming a plastic strain-rate vector normal to the von Mises yield surface and isotropic hardening/softening, which requires stress to increase/decrease uniformly in all directions. [32]

For single-limb stance loading displacement was incrementally applied to nodes in a 3-cm-diameter region on the femoral head and directed at 20° to the shaft axis in the coronal plane,

and the distal end of the proximal femur was fully constrained. For the nonlinear model of the fall loading condition, displacement was incrementally applied to nodes in a 3-cm-diameter region on the femoral head at 35° to the coronal plane and at 80° to the shaft axis with motion allowed transversely. Constraints were applied to nodes on the surface of the greater trochanter, over a thickness of 6 mm (two elements), to oppose the applied displacement while allowing for transverse motion. Note that these angles are measured within the plane containing the displacement vector and the shaft axis which does not coincide with any anatomic plane and results in an oblique, posterolateral loading condition. For the linear fall model, instead of applying displacement, a standard force of 1000 N, in the same direction as the displacement in the nonlinear models, was applied uniformly over the same nodes on the femoral head. Elements on the femoral head or greater trochanter that contained nodes to which force, displacement, or constraints were applied were assigned an elastic modulus of 20 GPa and a strength of 200 MPa to prevent severe element distortion. Nodes on the distal end of the model were fully restrained.

Finite element analysis was performed using with ABAQUS v. 6.6-3 (Dassault Systèmes Simulia Corp.). The nonlinear models used the geometric nonlinearity and automatic time-stepping options. For each increment of displacement, element strain and then stress were computed using the individual element's stress-strain relationship, in conjunction with the distortion energy yield criterion, which enabled the resultant reaction force at the femoral head to be computed. The computed reaction force for each increment of displacement produced a force-displacement curve analogous to a force-displacement curve during a mechanical testing experiment. Thus, the proximal femoral load capacity was defined as the maximum reaction force on the femoral head. For the linear fall FE models, the fall yield load was defined as the force at which 15 contiguous nonsurface elements exceeded their respective yield strengths [22]. Model linearity enabled this force to be determined from the element von Mises stress for the 1000 N applied load simply by scaling the model results.

Statistics

The data for men and women were first analyzed separately using descriptive statistics (Sigmastat/Sigmaplot, Systat Software, Inc.). To evaluate the relationship between FE strength and age and to test for sex differences, the data for men and women were analyzed together in a single model and multiple linear regression analysis was performed. The logarithm of FE-computed bone strength measures served as the dependent variable when necessary to ensure a normal distribution of residuals about the regression line. We did not evaluate additional strength-related dependent variables, such as an estimated factor of safety (proximal femur strength divided by the applied force) for each loading condition because we found previously (in unpublished work) that parameters normalized by body weight, height or combinations thereof did not affect fracture predictions. We did not control for height or weight because, in our previous work, the relationship between fracture status and FE strength was independent of height and weight [14,18]. An interaction between age and sex was considered in the regression analyses after centering age on the mean age of all subjects. This interaction was retained if it was significant at the alpha=0.1 level. Results were considered significant when $p<0.05$.

Comparative Data

To relate the FE results from the Mayo cohort to information about hip fracture, we supplemented these results with the FE-computed strength data from the hip fracture (45 men, 72 women) and control (94 men, 145 women) subjects of the AGES study [14,18]. This work involved prospective QCT scans of 5500 subjects, age 67 to 93 years, who were followed for 4 to 7 years. The FE-computed fracture loads for the AGES and Mayo cohorts, which used identical FE modeling methods, were graphed together to enable FE-computed fracture loads for male and female adults of all ages to be related to those of hip fracture in older subjects. We calculated the 50^{th}, 75^{th} and 100^{th} percentiles for each type of FE measure in the fracture group and showed those values on the graphs to assist with interpretation.

Results

The 397 FE models consisted of 5804 to 15371 nodes and 4504 to 12677 elements, reflecting the variation in subject size. The CT scanner cross-calibration equation that converted QCT density data from ρ_K on the Mayo scanner to ρ_{CHA} on the AGES scanner was ρ_{CHA} (g/cm^3) = 1.14 ρ_K − 0.017. The maximum elastic modulus in this cohort was 27.5 GPa, reflecting the young age of the subjects. The FE results and subject characteristics are summarized in Table 2, along with comparable data from the AGES cohort. The nonlinear FE models of one female and one male subject did not reach a peak load when subjected to the fall loading condition, resulting in missing data during the statistical analysis.

Table 2. Summary of Mayo cohort subjects and FE model results: Mean ± SD (range)

	Male		Female	
Age (years)	59.9 ± 16.6	(28 − 90)	60.9 ± 14.5	(27 − 90)
Height (cm)	176.3 ± 7.2	(157.0 − 195.4)	162.3 ± 6.1	(148.5 − 179.2)
Weight (kg)	90.2 ± 16.5	(53.0 − 134.0)	74.4 ± 15.4	(51.0 − 128.5)
Stance_LC (N)	10943 ± 3101	(3722 − 18969)	8456 ± 2735	(2617 − 18258)
Fall_LC (N)	3966 ± 678	(2305 − 6303)	3256 ± 614	(1717 − 5308)
Fall_yield (N)	1601 ± 637	(434 − 3871)	1229 ± 530	(280 − 2975)

Table 3. Summary of AGES cohort subjects and FE model results: Mean ± SD (range)[a]

	Male		Female	
	Control	Hip Fracture	Control	Hip Fracture
Age (years)	79.6 ± 5.2 (70 – 90)	80.0 ± 5.6 (71 – 93)	79.3 ± 5.7 (67 – 92)	79.5 ± 5.9 (67 – 93)
Height (cm)	174.9 ± 6.6 (162.4 – 190.5)	174.6 ± 5.9 (159.2 – 187.1)	159.2 ± 5.6 (139.3 – 173.0)	159.6 ± 6.1 (145.1 – 173.4)
Weight (kg)	82.6 ± 14.8 (52.4 – 135.0)	79.1 ± 13.9 (50.3 – 114.0)	68.3 ± 13.7 (37.2 – 112.0)	64.5 ± 15.1 (39.2 – 111.2)
Stance_LC (N)	10587 ± 2949 (4772 – 21784)	8081 ± 2011 (3123 – 12898)	7220 ± 2348 (2978 – 16330)	6024 ± 1575 (3085 – 10675)
Fall_LC (N)	3839 ± 564.0 (2408 – 5499)	3281 ± 539.2 (1723 – 4269)	2954 ± 555.8 (1816 – 4535)	2688 ± 435 (1700 – 4419)
Fall_yield (N)	1692 ± 671 (638 – 4257)	1226 ± 476 (276 – 2254)	1008 ± 476 (314 – 3071)	844 ± 333 (353 – 1945)

[a] Data obtained from [14] except for Fall_yield, which was from [18]

The FE-computed proximal femoral strengths were associated with age (Age, years), centered age (cAge = Age – 60.44 years) and sex (Figure 1) through the following equations, where Sex=0 for women and 1 for men:

- Log_{10}[Stance_LC (N)] = 3.907 + 0.111 Sex – 0.00560 cAge + 0.00151 Sex × cAge

  R^2=0.405; standard error of the estimate (SEE) = 0.116
- Fall_LC (N) = 4435 + 690.9 Sex – 19.40 Age

  R^2=0.399; SEE=571.067
- Log_{10}[Fall_yield (N)] = 3.051 + 0.115 Sex – 0.00695 cAge + 0.00309 Sex × cAge

  R^2=0.270; SEE=0.173

All constants and coefficients except those of the interactions were significant at the $p<0.001$ level and indicate that, at 60.44 years of age (cAge=0), Stance_LC, Fall_LC and Fall_yield were 23% (2351 N), 14% (691 N) and 23% (341 N) less in women than in men, respectively. Interactions between Sex and cAge were identified for Log_{10}(Stance_LC) ($p=0.045$) and Log_{10}(Fall_yield) ($p=0.006$), indicating that, when subjects 70 years of age were compared with same-sex subjects 10 years younger, Stance_LC was 13.8% lower in women and 9.9% lower in men, and Fall_yield was 17.4% lower in women and 9.3% lower in men. For Fall_LC, there was no interaction between sex and age ($p=0.35$), so Fall_LC was 19.4 N lower per year of age in both sexes, or 5.9% lower per 10 years of age in women compared with 4.9% in men. Between age 30 and 70 years, the average effects of age on Stance_LC, Fall_LC and Fall_yield were, respectively, 108 N, 19.4 N and 14.4 N lower per year in men and 120 N, 19.4 N and 21.6 N lower per year in women.

Discussion

The purpose of this study was to provide reference data and guidance to facilitate interpretation of CT scan-based FE-computed proximal femoral strengths of adult male and female subjects of all ages. Our results from the Mayo cohort constitute reference data for FE-computed proximal femoral strengths for subjects age 27 to 90 years. These reference data allow direct comparison of patient load capacity in stance and fall loading and fall yield load with those of this cohort. However, these reference data alone are not sufficient to determine if a subject is at long-term risk of fracture. To provide a more complete evaluation, these reference data need to be considered along with FE-computed strength values for hip fracture subjects. To facilitate this goal, while acknowledging the limitations described below, we combined the results for the Mayo cohort with those of the AGES cohort, using identical methodologies and cross-calibration of imaging hardware.

The computed load capacities indicate the minimum force required to cause a complete fracture (collapse) of the proximal femur and are associated with incident hip fracture in both men and women. Of the two load capacities, the stance load capacity is most strongly associated with fracture in both men and women. The reductions in strength associated with fracture in stance loading, 2377 N (22%) in men and 975 N (14%) in women, are respectively greater than those in fall loading, 484N (13%) in men and 206 N (7%) in women. The reductions in strength associated with fracture in each loading condition are also considerably greater in men than in women, indicating that identifying patients at risk of fracture is much more difficult in women than in men. In men, but not women, the fall load capacity is associated with incident hip fracture after accounting for areal BMD [14].

We included the fall yield load in this study even though yield load is not as strong a predictor of fracture as load capacity because yield load may be a more sensitive measure for evaluating changes in trabecular bone. In our models, fracture under fall loading begins in the trabecular bone [33], which is reflected most strongly by the fall yield load. Therefore, decreases in the yield load of an individual may be an early indicator of declining load capacity and future increases in hip fracture risk. Fall yield load may also be useful for evaluating interventions that affect trabecular bone, such as exercise [34-35].

Although comparisons between the Mayo and AGES cohorts must be made cautiously, the 100th percentiles for the stance load capacity (12.9 kN in men and 10.7 kN in women) and fall load capacities (4.3 kN in men and 4.4 kN in women) may be used as conservative thresholds to indicate that a patient is at high risk of fracture. However, the load capacities for fracture and non-fracture subjects in the AGES cohort overlap, making it difficult to set a less conservative value. This overlap occurs because subjects with low FE-computed load capacities who are at high risk of fracture do not always encounter forces that exceed the load capacity. This is especially true in older women because the load capacity in fracture and control subjects is identical in the oldest women [14]. Setting a threshold below which a patient is deemed at risk

of fracture is inherently subjective, which is why we have included several percentiles for the AGES cohort in Figure 1. Although we have included separate graphs for men and women, it is not clear whether men and women should have different fracture thresholds considering the substantial overlap between female fracture and control subjects in the AGES.

For evaluating subjects above age 70, proximal femoral strengths can be compared with those of both the Mayo and AGES cohorts, and the percentiles in the AGES hip fracture group may be used to guide an assessment of fracture risk. However, to evaluate younger subjects, the effect of aging must be considered. The results for the Mayo cohort provide relationships between the proximal femoral strengths and age that can be used to estimate where an individual may fall relative to the AGES cohort percentiles. That said, these estimates must be made with caution because our data are from a cross-sectional study and because some of the Mayo cohort received medications that could affect bone. That said, in the Mayo cohort, the stance load capacity in male and female subjects 30 to 90 years of age demonstrated a cross-sectional decrease of 108 N/y and 120 N/y, respectively, which were similar to those we reported previously in older subjects, 90 N/y and 134 N/y, respectively, in a longitudinal cohort of non-fracture subjects from the AGES Reykjavik study [5], indicating that these estimates appear reasonable. Fall load capacity was not included in the previous study, but fall yield load decreased much faster in the older subjects of the AGES longitudinal study, 24.4 N/y in men and 32.8 N/y in women, than in the Mayo cross-sectional cohort, 19.4 N/y in both sexes. This finding may indicate that that fall yield load decreases with age faster in older than in younger subjects and may reflect the greater sensitivity of fall yield load to trabecular bone status compared with stance load capacity.

The data presented in Figure 1 represent criteria for evaluating proximal femoral strengths, and potentially hip fracture risk, that are more robust than DXA measures because FE models can account for structural features that cannot be detected by DXA. Although osteoporotic levels of DXA areal BMD, with total hip BMD T-scores below < -2.5, are strongly

associated with increased risk of hip fracture [3], DXA is a poor predictor of hip fracture in patients with T-scores in the non-osteoporotic range. For example, Wainwright et al. [4] showed that, of 243 hip fracture patients from a cohort of 8065 women, more than half had DXA total hip BMD T-scores above −2.5 and 6% had T-scores greater than −1.0. Fundamentally, DXA cannot be a reliable method for evaluating hip fracture risk because it cannot incorporate key structural features that influence proximal femoral strength. For example, significant cortical thinning of the femoral neck and associated changes in cortical/trabecular geometry occur with age but are only weakly reflected by changes in DXA areal BMD [10,36]. As a result, reductions in DXA areal BMD tend to understate age-related reductions in proximal femoral strength [5,37] and associated increases in hip fracture risk [14].

Our previous report [19] illustrates the relationships between DXA T-scores and our load capacities for the Mayo cohort. These relationships clearly show that many of the Mayo subjects with T-scores between −2.5 and −1.0 have load capacities well below the 75th percentiles and may therefore be at risk of hip fracture. Amin et al. [1] suggested using FE analysis to evaluate individuals with DXA T-scores between −2.5 and −1.0. This approach is reasonable considering the advantages of finite element analysis over DXA for evaluating the structural integrity of the proximal femur.

An important limitation of this study is that the Mayo cohort is 97% Caucasian, representing the overall population of the Rochester area, and the AGES cohort is entirely Caucasian. Therefore, the results from these studies are applicable to Caucasians but should be used with caution when evaluating other races/ethnicities. Additionally, 33% of the Mayo cohort subjects were obese, which was not the case in the AGES cohort. Therefore, the percentiles for the AGES fracture group may not reflect obese subjects, including those in the Mayo cohort. Some subjects in the Mayo cohort also received medications that could have decreased or increased hip fracture risk. In the AGES cohort, the effect of medications did not significantly influence the association between FE model results and fracture incidence, so

comparisons between subjects taking medications and the AGES cohort are valid. Finally, some subjects in the Mayo cohort may have had or will have hip fractures as they age. We did not identify subjects who fractured because low trauma fractures were not distinguished from high trauma fractures and because the rate of hip fracture in a group this small produces relatively few hip fractures. Therefore, the Mayo cohort should be considered representative of a Caucasian population, whose risk of hip fracture is similar to that of the population in the Rochester area, and who may be obese and/or take medications that affect fracture risk.

Another limitation is that QCT data for the Mayo and AGES cohorts were obtained on two different CT scanners using different calibration phantoms. We addressed this limitation by cross-calibrating the CT scanners and calibration phantoms using a specially designed anthropometric calibration phantom [23]. Although cross-calibrating is inherently imperfect because phantoms do not always reflect the way the CT scanner depicts body habitus and tissue composition, our anthropometric phantom incorporated the human body shape and beam hardening effect of the pelvic bone structure, and has been previously validated, so the effect of using different scanners and phantoms was minimized. That said, the impact and importance of this cross-calibration was not trivial and should be considered when comparing these data with data from other scanners. Prior to cross-calibration, the FE results from the Mayo and AGES cohorts differed substantially. We had originally accounted for the different calibration phantoms by using a relationship, $\rho_{ash}=1.22\rho_K + 0.0526$ [38], to calculate ash density from ρ_K. This relationship was obtained from a different make and model of CT scanner (GE 9800 Research Scanner) and a different K_2HPO_4 calibration phantom than used in the present study, which led to Stance_LC, Fall_LC and Fall_yield values in the Mayo cohort that exceeded the results presented here by 37% (31% to 40%), 11% (−3% to 26%) and 32% (22% to 38%), respectively. Ultimately, the cross-calibration equation between the Mayo and AGES scanners, ρ_{CHA} (g/cm^3) = 1.14 ρ_K − 0.017 for 120 kVp was similar to equations obtained by Faulkner et al. [39] for 140 kVp, ρ_{CHA} (g/cm^3) = 1.18 ρ_K − 0.002, and for 80 kVp, ρ_{CHA} (g/cm^3) = 1.14 ρ_K − 0.004 (obtained

on a GE 9800 Research Scanner). Despite the similarity, even a 4% difference in slope can lead to a greater difference in mechanical properties due to the nonlinear density-property relationships, so cross-calibration using the actual scanners and phantoms is essential to obtain valid comparisons.

The quantitative results of this study are specific to the FE modeling method that was used [US Patent No. 9,245,069][24]. For example, the fall load capacities reported by Amin et al. [1] and Keaveny et al. [37] were notably greater than those found here, and the annual cross-sectional decreases in proximal femoral strength, 55 N/y and 61 N/y in men and women [37], respectively, were about triple those found here, despite being from a closely related cohort. These differences can be attributed to the substantial differences in FE methodologies of the studies. The importance of differences between the CT-based FE methodologies used by various investigators and the need to address them was recently discussed by Lee et al. [40]. To our knowledge, the FE modeling method used in the present study is the only one that computes stance and fall load capacities, the maximum forces that the proximal femur can support during single-limb stance and a fall onto the posterolateral aspect of the greater trochanter. Introducing this methodology dramatically improved the precision of FE-computed strengths in stance loading [41] and we more recently implemented this method for posterolateral fall loading as well [14]. Most other proximal femur FE modeling methods predict that ever-increasing forces and displacements can be applied to the femoral head and cannot represent collapse of the bone during fracture [1,12,15,37,42]. Our models also employ a posterolateral fall loading condition, which provides lower fracture forces than lateral fall loading [1,16] that are more strongly associated with fracture in men [14]. Differences between FE modeling methods [36,40] with respect to loading conditions, complex nonlinear mechanical properties, failure theories, and the precise definition of proximal femoral strength can affect the ability of the model to reflect the actual mechanical behavior of the proximal femur and the force of fracture. Therefore, comparisons with the results presented here must be made with care.

In conclusion, the Mayo cohort represents a reference database for FE-computed proximal femoral strengths of Caucasian adult men and women of all ages. The relationship between FE-computed strength and hip fracture can be examined through comparison with the FE data from the AGES cohort of older fracture and control subjects which were analyzed using identical methods and cross-calibration of imaging hardware. To evaluate long-term sufficiency of proximal femoral strengths in younger subjects, future decreases in bone strength due to aging can be estimated from the Mayo cohort data, and the projected bone strengths can be cautiously compared with those of the AGES cohort. Although strict criteria for identifying subjects at risk of fracture based on FE-calculated proximal femoral strengths have not been identified, these data may be useful for establishing criteria in future.

References

1. Amin S, Kopperdhal DL, Melton LJ 3rd, Achenbach SJ, Therneau TM, Riggs BL, Keaveny TM, Khosla S. Association of hip strength estimates by finite-element analysis with fractures in women and men. J Bone Miner Res. 2011 Jul;26(7):1593-600. doi: 10.1002/jbmr.347.
2. Liu J, Curtis EM, Cooper C, Harvey NC. State of the art in osteoporosis risk assessment and treatment. J Endocrinol Invest. 2019 Oct;42(10):1149-1164.
3. Marshall D, Johnell O, Wedel H. Meta-analysis of how well measures of bone mineral density predict occurrence of osteoporotic fractures. BMJ. 1996 May 18;312(7041):1254-9.
4. Wainwright SA, Marshall LM, Ensrud KE, Cauley JA, Black DM, Hillier TA, Hochberg MC, Vogt MT, Orwoll ES; Study of Osteoporotic Fractures Research Group. Hip fracture in women without osteoporosis. J Clin Endocrinol Metab. 2005 May;90(5):2787-93. Epub 2005 Feb 22.
5. Lang TF, Sigurdsson S, Karlsdottir G, Oskarsdottir D, Sigmarsdottir A, Chengshi J, Kornak J, Harris TBS, G., Jonsson BY, Siggeirsdottir K, Eiriksdottir G, Gudnason V, Keyak JH. Age-related loss of proximal femoral strength in elderly men and women: the Age Gene/Environment Susceptibility Study – Reykjavik. Bone 2012;50: 743-748.

6. Sibonga JD, Spector ER, Keyak JH, Zwart SR, Smith SM, Lang TF. Use of Quantitative Computed Tomography to Assess for Clinically-relevant Skeletal Effects of Prolonged Spaceflight on Astronaut Hips. J Clin Densitom. 2019 Aug 26. pii: S1094-6950(19)30121-0. doi: 10.1016/j.jocd.2019.08.005. [Epub ahead of print]
7. Yang L, Burton AC, Bradburn M, Nielson CM, Orwoll ES, Eastell R; Osteoporotic Fractures in Men (MrOS) Study Group. Distribution of bone density in the proximal femur and its association with hip fracture risk in older men: the osteoporotic fractures in men (MrOS) study. J Bone Miner Res. 2012 Nov;27(11):2314-24. doi: 10.1002/jbmr.1693.
8. Yang L, Udall WJ, McCloskey EV, Eastell R. Distribution of bone density and cortical thickness in the proximal femur and their association with hip fracture in postmenopausal women: a quantitative computed tomography study. Osteoporos Int. 2014 Jan;25(1):251-63. doi: 10.1007/s00198-013-2401-y. Epub 2013 May 30.
9. Cheng X, Li J, Lu Y, Keyak J, Lang T. Proximal femoral density and geometry measurements by quantitative computed tomography: association with hip fracture. Bone. 2007 Jan;40(1):169-74. Epub 2006 Jul 28. PMID: 16876496
10. Johannesdottir F, Aspelund T, Reeve J, Poole KE, Sigurdsson S, Harris TB, Gudnason VG, Sigurdsson G. Similarities and differences between sexes in regional loss of cortical and trabecular bone in the mid-femoral neck: the AGES-Reykjavik longitudinal study. J Bone Miner Res. 2013 Oct;28(10):2165-76. doi: 10.1002/jbmr.1960.
11. Cody DD, Gross GJ, Hou FJ, Spencer HJ, Goldstein SA, Fyhrie DP. Femoral strength is better predicted by finite element models than QCT and DXA. J Biomech 1999;32: 1013-1020.
12. Johannesdottir F, Thrall E, Muller J, Keaveny TM, Kopperdahl DL, Bouxsein ML. Comparison of non-invasive assessments of strength of the proximal femur. Bone. 2017 Dec;105:93-102. doi: 10.1016/j.bone.2017.07.023. Epub 2017 Jul 21.

13. Pottecher P, Engelke K, Duchemin L, Museyko O, Moser T, Mitton D, Vicaut E, Adams J, Skalli W, Laredo JD, Bousson V. Prediction of Hip Failure Load: In Vitro Study of 80 Femurs Using Three Imaging Methods and Finite Element Models-The European Fracture Study (EFFECT). Radiology. 2016 Sep;280(3):837-47.
14. Keyak JH, Sigurdsson S, Karlsdottir GS, Oskarsdottir D, Sigmarsdottir A, Kornak J, Harris TB, Sigurdsson G, Jonsson BY, Siggeirsdottir K, Eiriksdottir G, Gudnason V, Lang TF. Effect of finite element model loading condition on fracture risk assessment in men and women: the AGES-Reykjavik study. Bone. 2013 Nov;57(1):18-29. doi: 10.1016/j.bone.2013.07.028. Epub 2013 Jul 29.
15. Kopperdahl DL, Aspelund T, Hoffmann PF, Sigurdsson S, Siggeirsdottir K, Harris TB, Gudnason V, Keaveny TM. Assessment of incident spine and hip fractures in women and men using finite element analysis of CT scans. J Bone Miner Res. 2014 Mar;29(3):570-80. doi: 10.1002/jbmr.2069.
16. Orwoll ES, Marshall LM, Nielson CM, Cummings SR, Lapidus J, Cauley JA, Ensrud K, Lane N, Hoffmann PR, Kopperdahl DL, Keaveny TM. Finite element analysis of the proximal femur and hip fracture risk in older men. J Bone Miner Res 2009;24: 475-483.
17. Johannesdottir F, Allaire B, Bouxsein ML. Fracture Prediction by Computed Tomography and Finite Element Analysis: Current and Future Perspectives. Curr Osteoporos Rep. 2018 Aug;16(4):411-422. doi: 10.1007/s11914-018-0450-z.
18. Keyak JH, Sigurdsson S, Karlsdottir G, Oskarsdottir D, Sigmarsdottir A, Zhao S, Kornak J, Harris TBS, G., Jonsson BY, Siggeirsdottir K, Eiriksdottir G, Gudnason V, Lang TF. Male-female differences in the association between incident hip fracture and proximal femoral strength computed by finite element analysis. Bone 2011;48: 1239-1245.
19. Michalski AS, Amin S, Cheung AM, Cody DD, Keyak JH, Lang TF, Nicolella DP, Orwoll ES, Boyd SK, Sibonga JD. Hip load capacity cut-points for Astronaut Skeletal Health NASA Finite Element Strength Task Group Recommendations. NPJ Microgravity. 2019 Mar 14;5:6.

20. Riggs BL, Melton Iii LJ 3rd, Robb RA, Camp JJ, Atkinson EJ, Peterson JM, Rouleau PA, McCollough CH, Bouxsein ML, Khosla S. Population-based study of age and sex differences in bone volumetric density, size, geometry, and structure at different skeletal sites. J Bone Miner Res. 2004 Dec;19(12):1945-54. Epub 2004 Sep 20.
21. Keyak JH, Kaneko TS, Tehranzadeh J, Skinner HB. Predicting proximal femoral strength using structural engineering models. Clin Orthop Relat Res. 2005 Aug;(437):219-28.
22. Keyak JH, Rossi SA, Jones KA, Skinner HB. Prediction of femoral fracture load using automated finite element modeling. J Biomech 1998;31: 125-133.
23. Bonaretti S, Carpenter RD, Saeed I, Burghardt AJ, Yu L, Bruesewitz M, Khosla S, Lang T. Novel anthropomorphic hip phantom corrects systemic interscanner differences in proximal femoral vBMD. Phys Med Biol. 2014 Dec 21;59(24):7819-34. doi: 10.1088/0031-9155/59/24/7819.
24. Keyak JH. Methods for Calculating Bone Fracture Load. 2016 Jan 26; US Patent No. 9,245,069.
25. Seitz P, Ruegsegger P: Fast contour detection algorithm for high precision quantitative CT. IEEE Trans Med Imag 1983; MI-2(3):136-41.
26. Keyak JH, Meagher JM, Skinner HB, Mote CD Jr. Automated three-dimensional finite element modelling of bone: a new method. J Biomed Eng. 1990 Sep;12(5):389-97.
27. Kaneko TS, Bell JS, Pejcic MR, Tehranzadeh J, Keyak JH. Mechanical properties, density and quantitative CT scan data of trabecular bone with and without metastases. J Biomech. 2004 Apr;37(4):523-30.
28. Kaneko TS, Pejcic MR, Tehranzadeh J, Keyak JH. Relationships between material properties and CT scan data of cortical bone with and without metastatic lesions. Med Eng Phys. 2003 Jul;25(6):445-54. Erratum in: Med Eng Phys. 2004 May;26(4):361.
29. Reilly DT, Burstein AH. The elastic and ultimate properties of compact bone tissue. J Biomech 1975;8:393–405.

30. Van Buskirk WC, Ashman RB. The elastic moduli of bone. Transactions of the American Society of Mechanical Engineers. J Appl Mech 1981;45:131–43.
31. Keyak JH, Lee IY, Nath DS, Skinner HB. Postfailure compressive behavior of tibial trabecular bone in three anatomic directions. J Biomed Mater Res 1996;31: 373-378.
32. Shames IH, Cozzarelli FA. Elastic and inelastic stress analysis. Englewood Cliffs, NJ: Prentice-Hall, 1992.
33. Keyak JH, Rossi SA, Jones KA, Les CM, Skinner HB. Prediction of fracture location in the proximal femur using finite element models. Med Eng Phys. 2001 Nov;23(9):657-64.
34. Fuchs RK, Kersh ME, Carballido-Gamio J, Thompson WR, Keyak JH, Warden SJ. Physical Activity for Strengthening Fracture Prone Regions of the Proximal Femur. Curr Osteoporos Rep. 2017 Feb;15(1):43-52. doi: 10.1007/s11914-017-0343-6.
35. Warden SJ, Carballido-Gamio J, Weatherholt AM, Keyak JH, Lang TF, Kersh ME, Fuchs RK: Heterogeneous spatial and strength adaptation of the proximal femur to physical activity: a within-subject controlled cross-sectional study. J Bone Miner Res. 2019 Dec 11. doi: 10.1002/jbmr.3939. [Epub ahead of print]
36. Bouxsein ML, Zysset P, Glüer CC, McClung M, Biver E, Pierroz DD, Ferrari SL; IOF Working Group on Hip Bone Strength as a Therapeutic Target. Perspectives on the non-invasive evaluation of femoral strength in the assessment of hip fracture risk. Osteoporos Int. 2020 Jan 3. doi: 10.1007/s00198-019-05195-0. [Epub ahead of print]
37. Keaveny TM, Kopperdahl DL, Melton LJ, 3rd, Hoffmann PF, Amin S, Riggs BL, Khosla S. Age-dependence of femoral strength in white women and men. J Bone Miner Res 2010;25: 994-1001.
38. Les CM, Keyak JH, Stover SM, Taylor KT, Kaneps AJ. Estimation of material properties in the equine metacarpus with use of quantitative computed tomography. J Orthop Res. 1994 Nov;12(6):822-33.

39. Faulkner KG, Glüer CC, Grampp S, Genant HK. Cross-calibration of liquid and solid QCT calibration standards: corrections to the UCSF normative data. Osteoporos Int. 1993 Jan;3(1):36-42.
40. Lee Y, Ogihara N, Lee T. Assessment of finite element models for prediction of osteoporotic fracture. J Mech Behav Biomed Mater. 2019 Sep;97:312-320.
41. Keyak JH. Improved prediction of proximal femoral fracture load using nonlinear finite element models. Med Eng Phys. 2001 Apr;23(3):165-73. Erratum in: Med Eng Phys. 2003 Sep;25(7):615.
42. Adams AL, Fischer H, Kopperdahl DL, Lee DC, Black DM, Bouxsein ML, Fatemi S, Khosla S, Orwoll ES, Siris ES, Keaveny TM. Osteoporosis and Hip Fracture Risk From Routine Computed Tomography Scans: The Fracture, Osteoporosis, and CT Utilization Study (FOCUS). J Bone Miner Res. 2018 Jul;33(7):1291-1301. doi: 10.1002/jbmr.3423. Epub 2018 Apr 17.

Acknowledgments

This work was supported by NIH/NIA R01AG028832, NIH/NIAMS R01AR46197, NIH/NIAMS R01AR060700, NIH/NIAMS R01AR064140, by NIH/NIAMS grants AR-27065 and M01 RR00585 and by NASA grants NNJ04HC7SA, NNJ04HF78G, NNJ12HC91P. This study was made possible by the Rochester Epidemiology Project. We thank Dr. Vilmundur Gudnason (Faculty of Medicine, School of Health Sciences, University of Iceland, Reykjavik, Iceland) for the opportunity to include data from the AGES cohort. The Age, Gene/Environment Susceptibility Reykjavik Study was funded by NIH contract N01-AG-12100, the NIA Intramural Research Program, Hjartavernd (the Icelandic Heart Association), and the Althingi (the Icelandic Parliament) and was approved by the Icelandic National Bioethics Committee (VSN: 00-063) and the Data Protection Authority. The authors appreciate the assistance of Donald J. Roth, Ph.D. of the NASA Glenn Research Center, Cleveland, OH who wrote software to convert the Mayo Cohort CT scans from 2-mm to 3-mm-thick slices. The researchers are indebted to the participants in Rochester, MN, USA and Reykjavik, Iceland for their willingness to participate in these studies.

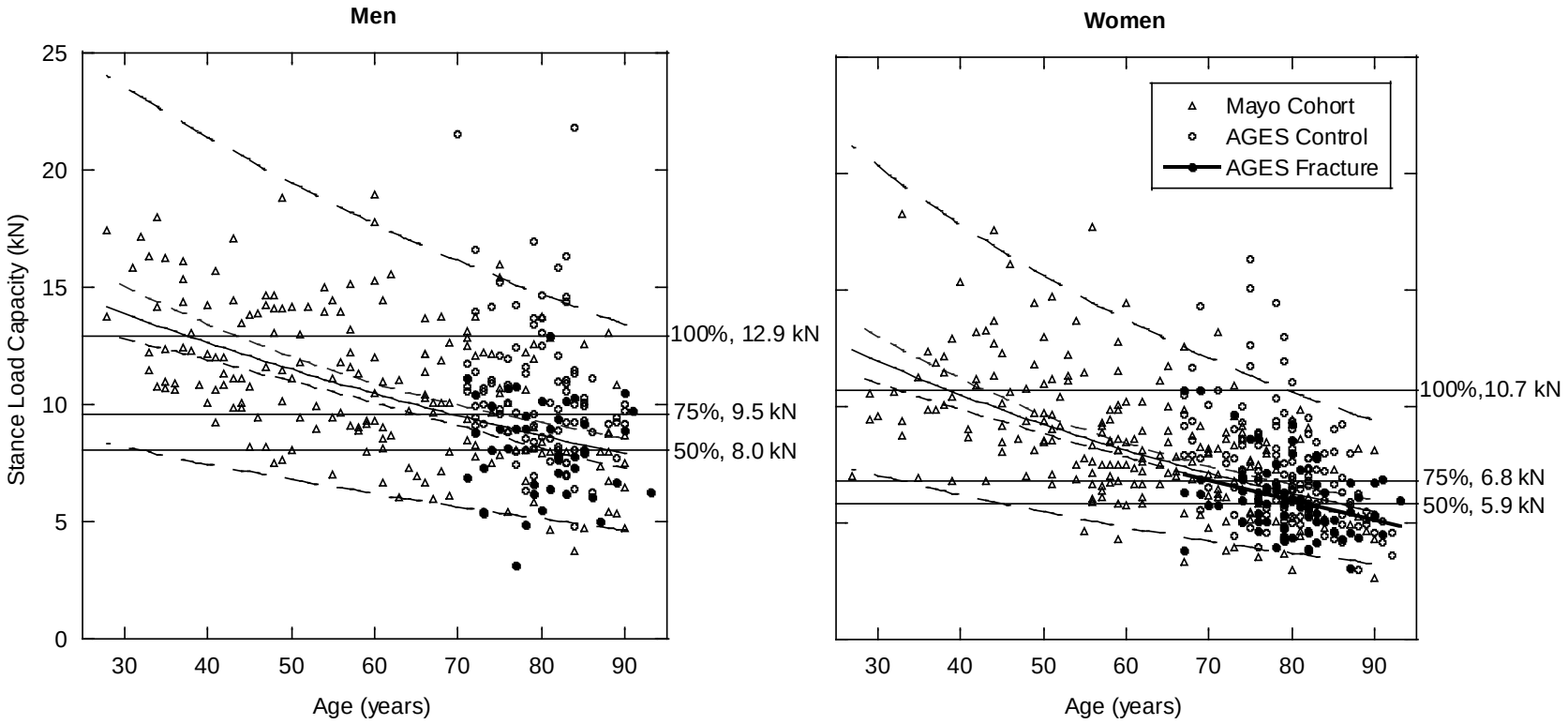

(a)

Figure 1. Computed load capacities in single-limb stance (a) and posterolateral fall loading (b), and computed yield load in posterolateral fall (c) for the Mayo and AGES cohorts versus age in men (left) and women (right). In each graph, the Mayo cohort regression line, 95% confidence interval for the regression line, and 95% confidence interval for the population are indicated by a solid line, short dashed lines and long dashed lines, respectively. The 50th, 75th and 100th percentiles for men (left) and women (right) in the AGES fracture group are indicated. Regression lines between FE strength and age in the AGES fracture group were significant only for women and are shown only in the graphs on the right (heavy solid lines).

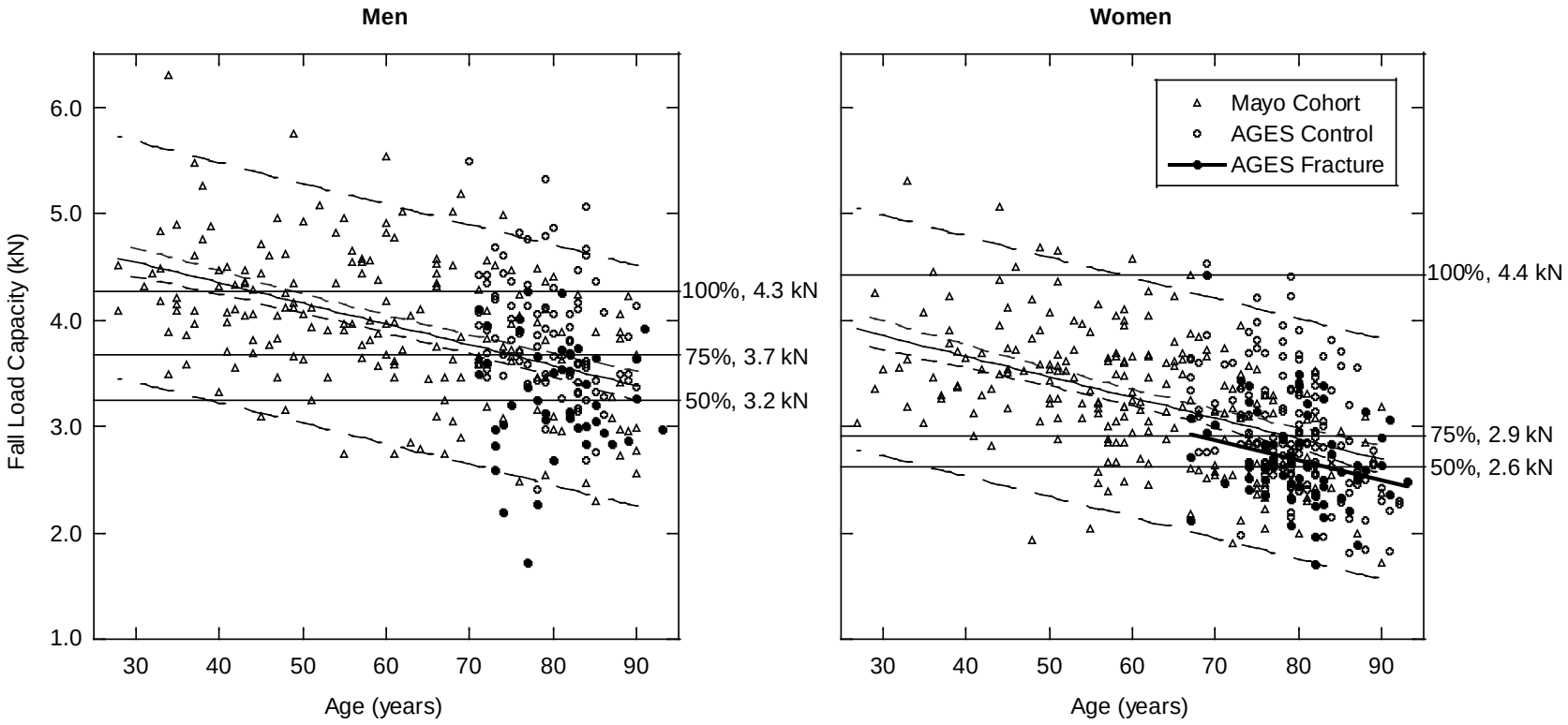

(b)

Figure 1. Computed load capacities in single-limb stance (a) and posterolateral fall loading (b), and computed yield load in posterolateral fall (c) for the Mayo and AGES cohorts versus age in men (left) and women (right). In each graph, the Mayo cohort regression line, 95% confidence interval for the regression line, and 95% confidence interval for the population are indicated by a solid line, short dashed lines and long dashed lines, respectively. The 50th, 75th and 100th percentiles for men (left) and women (right) in the AGES fracture group are indicated. Regression lines between FE strength and age in the AGES fracture group were significant only for women and are shown only in the graphs on the right (heavy solid lines).

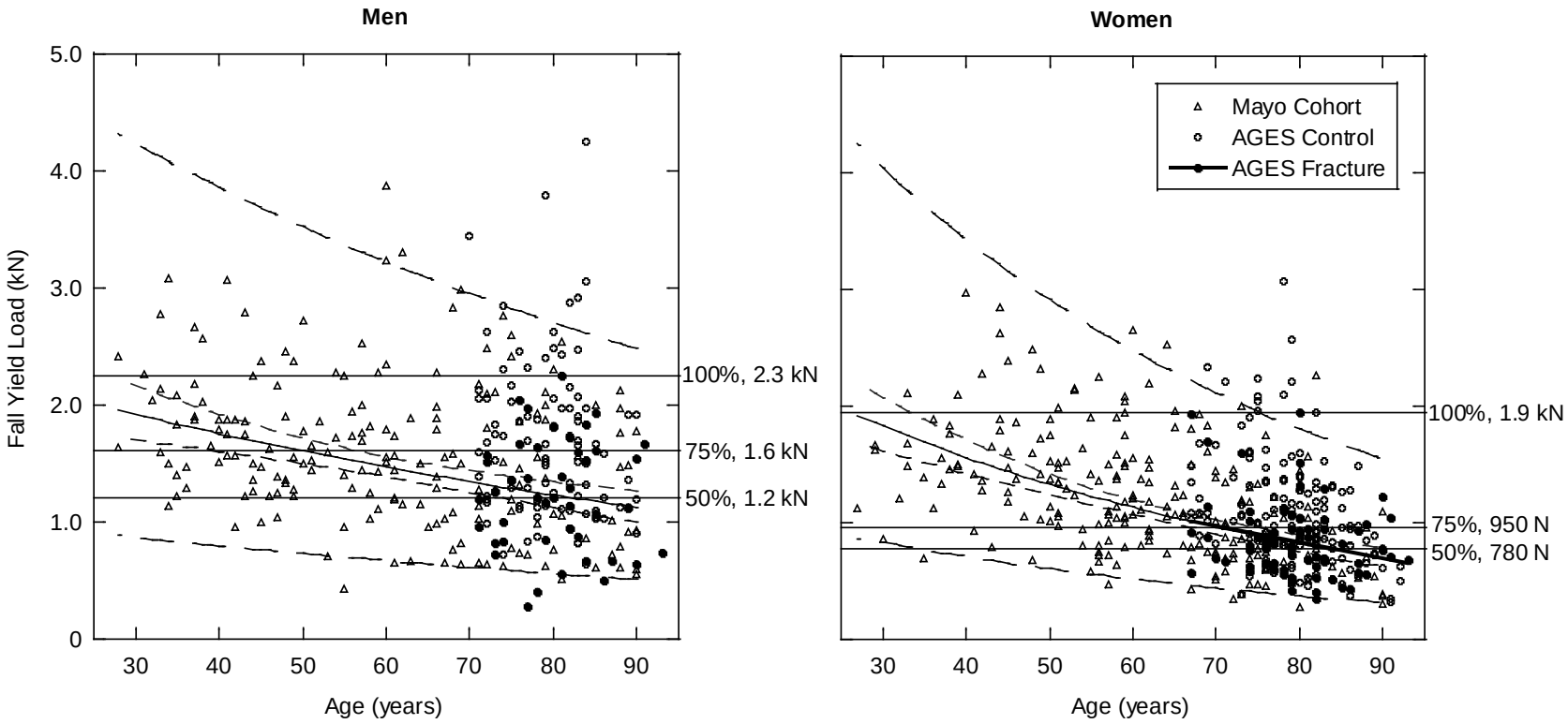

(c)

Figure 1. Computed load capacities in single-limb stance (a) and posterolateral fall loading (b), and computed yield load in posterolateral fall (c) for the Mayo and AGES cohorts versus age in men (left) and women (right). In each graph, the Mayo cohort regression line, 95% confidence interval for the regression line, and 95% confidence interval for the population are indicated by a solid line, short dashed lines and long dashed lines, respectively. The 50th, 75th and 100th percentiles for men (left) and women (right) in the AGES fracture group are indicated. Regression lines between FE strength and age in the AGES fracture group were significant only for women and are shown only in the graphs on the right (heavy solid lines).